

Solamargine induces apoptosis of human renal carcinoma cells via downregulating phosphorylated STAT3 expression

SHUAISHUAI HUANG¹, MINYI SUN¹, YU REN¹, TING LUO², XUE WANG¹, GUOBIN WENG¹ and DONG CEN²

¹Laboratory of Renal Carcinoma; ²Department of Medical Laboratory, Ningbo Yinzhou No. 2 Hospital, Urology and Nephrology Institute of Ningbo University, Ningbo, Zhejiang 315100, P.R. China

Received June 11, 2022; Accepted September 1, 2023

DOI: 10.3892/ol.2023.14080

Abstract. Solamargine (SM), an active compound derived from *Solanum nigrum*, triggers apoptosis and inhibits the metastatic and oxidative activities of various types of tumor cells. However, the effect of SM on human renal carcinoma cells remains unknown. In the present study, the molecular mechanisms underlying the antitumor effects of SM on ACHN and 786-O cells were elucidated. Specifically, MTT and colony formation assays were conducted to evaluate the impact of SM treatment on the proliferation of ACHN and 786-O cells, and flow cytometry was conducted to determine the influence of SM on the apoptosis rates of these cells. In addition, the expression of target proteins was determined by western blotting. The results revealed that SM not only inhibited cell viability but also promoted the apoptosis of ACHN and 786-O cells in a time- and dose-dependent manner. Moreover, treatment of ACHN and 786-O cells with SM significantly enhanced the caspase-3, caspase-8 and caspase-9 activities. Furthermore, SM downregulated the expression of phosphorylated signal transducer and activator of transcription-3 (p-STAT3) and Bcl-2 but increased the expression of cleaved caspase-3, -8, -9 and Bax. BAY2353, a p-STAT3 inhibitor, inhibited the viability of ACHN and 786-O cells, increased the expression of cleaved caspase-9 and Bax and decreased the expression of p-STAT3 and Bcl-2. Further experiments demonstrated that SM inhibited tumor growth in xenograft nude mice without causing specific toxicity to the major organs. Collectively,

these findings indicated that SM not only inhibited the viability but also promoted the apoptosis of ACHN and 786-O cells, through a mechanism involving downregulation of p-STAT3 expression.

Introduction

Renal cell carcinoma (RCC) accounts for 2-3% of all cancer cases, while clear cell RCC (ccRCC) accounts for ~75% of all RCC cases worldwide (1,2). It is estimated that 20-50% of patients who are diagnosed with localized RCC tumors will still encounter local recurrence or tumor metastasis after surgical resection, and that their 5-year survival rate is <10% (2,3). This therefore calls for the urgent development of effective and less toxic drugs for treating RCC tumors, and identifying the molecular targets and underlying mechanisms of RCC is an important step in developing these treatments. Signal transducer and activator of transcription (STAT) 3 is phosphorylated and activated by various hormones, growth factors and cytokines (4). Upon activation, phosphorylated STAT3 (p-STAT3) dimerizes and translocates to the nucleus, where it regulates transcription of a broad spectrum of target genes involved in the regulation of critical functions, including cell proliferation (5), apoptosis (6), metastasis (7), angiogenesis (8) and immune responses (9). Numerous studies have shown that high STAT3 levels were associated with the poor prognosis of patients with RCC (10-13). Notably, inhibition of STAT3 inhibited cell proliferation and induced the apoptosis of RCC cells (14), indicating that STAT3 could be a potential and effective target for RCC therapy.

Prospecting for novel anticancer agents derived from traditional Chinese medicine has gained research interest. Notably, the glycoalkaloid compound, solamargine (SM), the main active ingredient in *Solanum nigrum* L, was found to possess significant inhibitory effects against several types of cancer cells. For example, preliminary results from a number of studies have revealed its efficacy and potential underlying mechanisms of action against prostate cancer (15), hepatoma (16), melanoma (17) and ovarian cancer cells (18). However, to the best of our knowledge, the effect and underlying molecular mechanism of action of SM on human RCC cells remains unknown. Therefore, the main purpose of the present study was to investigate the effect of SM on

Correspondence to: Dr Guobin Weng, Laboratory of Renal Carcinoma, Ningbo Yinzhou No. 2 Hospital, Urology and Nephrology Institute of Ningbo University, 998 North Qianhe Road, Yinzhou, Ningbo, Zhejiang 315100, P.R. China
E-mail: ddwgbn@aliyun.com

Dr Dong Cen, Department of Medical Laboratory, Ningbo Yinzhou No. 2 Hospital, Urology and Nephrology Institute of Ningbo University, 998 North Qianhe Road, Yinzhou, Ningbo, Zhejiang 315100, P.R. China
E-mail: cendong2002@126.com

Key words: apoptosis, human renal carcinoma, solamargine, STAT3, viability

the viability and apoptosis of RCC cells, and to elucidate the underlying molecular mechanisms.

Materials and methods

Cell lines and culture. The ACHN cell line was obtained from The Cell Bank of Type Culture Collection of The Chinese Academy of Sciences, while the 786-O cell line was purchased from American Type Culture Collection. ACHN cells were cultured in DMEM (HyClone; Cytiva) and 786-O cells were cultured in 1640 medium (HyClone; Cytiva). The media were supplemented with 10% heat-inactivated fetal bovine serum (Shanghai ExCell Biology, Inc.), 100 U/ml penicillin and 100 mg/ml streptomycin (HyClone; Cytiva). Both cell lines were maintained in a humidified atmosphere at 37°C and 5% CO₂.

Drug and chemicals. SM was purchased from MedChemExpress (cat. no. HY-N0069) and dissolved in dimethyl sulfoxide (DMSO). The dose was prepared as a 10 mM stock solution (stored at -80°C) and freshly diluted to a final concentration using cell culture medium prior to use. BAY2353 was obtained from Selleck Chemicals.

Cell toxicity experiments. Cells were seeded in 96-well plates (Corning Inc.) containing culture media at a density of 2,000 cells/well and were cultured for a further 24 h. Then, the media was replaced with fresh media containing different SM concentrations (0, 0.1, 1.0, 10.0 and 100.0 μM) and incubated for a further 0, 24, 48 or 72 h, respectively. After incubation, 20 μl of MTT reagent (Promega Corporation) was added to each well, and the samples were incubated at 37°C for a further 20 min. The optical density was measured at 492 nm using a Multiskan GO spectrophotometer (Thermo Fisher Scientific, Inc.). The experiments were repeated three times.

Flow cytometry. The rate of cell apoptosis was analyzed using an Annexin V/propidium iodide (PI) apoptosis detection kit [Hangzhou MultiSciences (Lianke) Biotech, Co., Ltd.] according to the manufacturer's instructions. Briefly, cells were trypsinized, washed three times with PBS and then resuspended in 0.5 ml binding buffer containing 5 μl Annexin-V-FITC and 10 μl PI for 30 min at room temperature. Then, the contents were subjected to a FACSCalibur Flow Cytometer using CellQuest Pro software (Version 5.1, BD Biosciences). The experiments were repeated three times.

Detection of caspase activity. The activities of caspase-3, caspase-8 and caspase-9 in cells treated with SM were detected using the caspase activity assay kit, according to the manufacturer's instructions (Beyotime Institute of Biotechnology). Absorbance values were measured at 405 nm using a spectrophotometer (Multiscan skyhigh; Thermo Fisher Scientific, Inc.). The experiments were repeated three times.

Colony formation assay. Cells were seeded into 6-well plates at a density of 500 cells/well, then treated with 0, 0.05, 0.10 and 0.20 μM SM. The cells were then incubated for 15 days at 37°C and 5% CO₂, fixed with methanol solution for 15 min at room temperature, and finally stained with Giemsa

for 30 min at room temperature, and colonies consisting of ≥50 cells were manually counted. The experiments were repeated three times.

Fluorescence staining. Cells were first treated with either SM or 0.1% DMSO, washed with PBS and then fixed with 4% paraformaldehyde solution for 15 min at room temperature. Then, the cells were again washed with PBS and the chromosomes were stained with 5 μg/ml DAPI for 5 min at room temperature. Following staining, the cells were washed with PBS and then subjected to fluorescence microscopy (Nikon Corporation) for visualization and image capture. The experiments were repeated three times.

Western blot assay. RCC cells were treated with different doses of SM in 6-well plates, then total proteins were extracted using the RIPA Lysis Buffer (Beijing Solarbio Science & Technology Co., Ltd.). A cell nuclear and cytoplasmic protein extraction kit (Beyotime Institute of Biotechnology) was used to extract the nuclear and cytoplasmic proteins. Protein concentrations were determined using the BCA protein assay kit (Beyotime Institute of Biotechnology), then equal amounts of protein (25 μg) were separated on a 12% SDS-PAGE. The protein bands were subsequently transferred onto PVDF membranes (MilliporeSigma), which were then blocked for 1 h with 5% (w/v) not-fat dry milk at room temperature. The membranes were then incubated overnight with appropriate dilutions of the following primary antibodies at 4°C: Mouse monoclonal anti-Bax (cat. no. #89477; 1:1,000; Cell Signaling Technology, Inc.), mouse monoclonal anti-Bcl-2 (cat. no. 15071; 1:1,000; Cell Signaling Technology, Inc.), rabbit monoclonal anti-GAPDH (cat. no. 2118; 1:2,000; Cell Signaling Technology, Inc.), rabbit monoclonal anti-p-STAT3 (cat. no. 9145; 1:2,000; Cell Signaling Technology, Inc.), mouse monoclonal anti-total STAT3 (cat. no. 9139; t-STAT3; 1:1,000; Cell Signaling Technology, Inc.), rabbit monoclonal anti-cleaved caspase-3 (cat. no. 9664; 1:1,000; Cell Signaling Technology, Inc.), rabbit monoclonal anti-cleaved caspase-9 (cat. no. 7237; 1:1,000; Cell Signaling Technology, Inc.), rabbit monoclonal anti-Histone H3 (cat. no. 4499; 1:2,000; Cell Signaling Technology, Inc.) and rabbit monoclonal anti-cleaved caspase-8 (cat. no. 38680; 1:2,000; Invitrogen; Thermo Fisher Scientific, Inc.). Next, the membranes were washed three times with TBST (containing 1% Tween-20), then probed with a secondary HRP conjugated goat anti-mouse (cat. no. BA1050; 1:5000; Boster) or HRP conjugated goat anti-rabbit antibodies (cat. no. BA1054; 1:5000; Boster) for 1.5 h at room temperature. Finally, protein bands were visualized using enhanced chemiluminescence reagent (Advansta) and analyzed by Tanon Image software (Version 1.00, Tanon Science & Technology Co., Ltd., Shanghai, China). The experiments were repeated three times.

Mouse model. Male 6-week-old BALB/c nude mice were purchased from Shanghai SLAC Laboratory Animal Co., Ltd, and maintained in an air-conditioned specific pathogen-free room (temperature: 23±3°C; humidity: 40-65%) with a 12:12-h light-dark cycle. A total of 10 nude mice were randomly divided into two equal groups (5 per group), then tumors were induced by subcutaneously injecting ACHN cells (5.0×10⁶ cells/mice) into the right flank area of each

mouse on day 0. Mice in the experimental group were intragastrically administered 25 mg/kg SM once daily (19), while those in the control group were given PBS. The animal health and behavior was checked once a day. The initial average weight of the SM group and control group were 16.55 and 16.35 g respectively. The length of the experiment lasted one month. All ten nude mice eventually developed tumors during this period. Tumor growth and animal body weight were measured after every 3 days, and the size of the tumors were calculated using the following formula: $\pi/6 \times \text{length} \times \text{weight}^2$. At the end of the experiment, all mice were sacrificed through cervical dislocation after intraperitoneal injection of 2% sodium pentobarbital (25 mg/kg) anesthetic. Tumor tissues were collected and weighed prior to immunohistochemistry. The major organs (heart, liver, spleen, lung and kidney) were also collected.

Immunohistochemistry. Tumor tissues were fixed for 12 h with 4% paraformaldehyde at room temperature, cut into 4- μm sections and then embedded using paraffin. The slides were heated at 60°C for 1 h and deparaffinized in xylene solution, rehydrated by descending concentrations of ethanol, washed three times with PBS, blocked with 5% bovine serum albumin (cat. no. SW3015; Solarbio) at room temperature for 1 h, and then incubated with primary antibody against p-STAT3 (cat. no. 9145; 1:400; Cell Signaling Technology, Inc.) at room temperature for 1 h. Next, the sections were washed three times with PBS and incubated with Biotin-HRP labeled secondary antibody (cat. no. BA1018; 1:200; Boster) at room temperature for 1 h. The immunostained cells were counted from five randomly selected fields, viewed under x400 magnification using an inverted light microscope (Version ECLIPSE NI-U, Nikon Corporation). The number of positively stained cells was measured using the Image-Pro Plus analysis software (Version 6.0, Media Cybernetics).

Haematoxylin and eosin (H&E) staining. Paraffin-embedded sections were prepared as aforementioned, then stained with hematoxylin for 1 min at room temperature. The sections were washed for 10 min with water and then stained with eosin for 1 min at room temperature. The slides were visualized using an optical microscope under x100 magnification.

Statistical analysis. All statistical analyses were performed using SPSS version 18.0 (SPSS, Inc.) and GraphPad Prism version 5.0 (Dotmatics) software. Data are presented as the mean \pm standard deviation. The unpaired two-tailed Student's t-test was used to analyze the statistical difference between two groups. A one-way ANOVA analysis followed by Dunnett's test was used to calculate the statistical difference between multiple groups. $P < 0.05$ was considered to indicate a statistically significant difference.

Results

SM suppresses viability of RCC cells. The chemical structure of SM is shown in Fig. 1A. The results of the MTT assay demonstrated that SM inhibited the viability of both ACHN and 786-O cells in a dose- and time-dependent manner (Fig. 1B and C). A summary of the SM IC_{50} values in ACHN

Table I. IC_{50} values of solamargine in ACHN and 786-O cells.

Cell line	$\text{IC}_{50}, \mu\text{M}$			
	12 h	24 h	48 h	72 h
ACHN	6.888	0.895	0.311	0.105
786-O	5.190	1.124	0.527	0.249

and 786-O cells across each incubation period is shown in Table I. Moreover, SM treatment suppressed the clonogenicity of ACHN and 786-O cells (Fig. 2). Notably, the density and number of cell colonies significantly decreased with increasing SM concentrations.

SM induces the apoptosis of RCC cells. A previous study has demonstrated an association between inhibition of cell viability with the induction of apoptosis in cancer cells (20). To evaluate whether SM induces apoptosis, the nuclei of RCC cells were stained with DAPI. The nuclear chromatin condensation and fragmentation in cells were notably increased with increasing concentrations of SM (Fig. 3A). Next, the rate of SM-induced apoptosis was explored using an Annexin V/PI assay. The results of the assay demonstrated that SM treatment increased total cell apoptosis in a dose-dependent manner (Fig. 3B). Moreover, SM-treated cells exhibited higher rates of apoptosis at both the early and late stages compared with the control group, however this was not significant for early apoptosis. To elucidate the underlying mechanism of SM-induced apoptosis, the activities of caspase-3, caspase-8 and caspase-9 were determined. It was found that the activities of all three caspases were significantly upregulated at higher SM concentrations (Table II). In addition, the expression levels of cleaved caspase-3,-8,-9 and Bax were markedly upregulated while the level of Bcl-2 was downregulated following 24 h SM treatment (Fig. 4).

SM downregulates expression of p-STAT3 and inhibits its translocation into the cytoplasm. Accumulating evidence has underscored the critical role of STAT3 in modulating the viability and proliferation of cancer cells (21-23). Therefore, it was next determined whether STAT3 was involved in SM-induced cell apoptosis. It was found that SM mediated a significant reduction in the p-STAT3/t-STAT3 ratio in a dose-dependent manner (Fig. 5A and B). Phosphorylation of STAT3 is required for STAT3 dimerization, which enables it to translocate from the cytoplasm to the nucleus, thus regulating expression of its target genes (24,25). To further confirm the localization of p-STAT3, proteins from SM-treated RCC cells were fractionated using a nuclear and cytoplasmic protein extraction kit, following 24 h of treatment. The results demonstrated that SM treatment downregulated p-STAT3 levels in the nuclear fraction of RCC cells (Fig. 5C and D). In addition, treatment with the p-STAT3 inhibitor, BAY2353, inhibited the viability of ACHN and 786-O cells (Fig. 6A and B). Furthermore, BAY2353 increased the expression levels of cleaved caspase-9 and Bax but decreased levels of p-STAT3 and Bcl-2 (Fig. 6C-F).

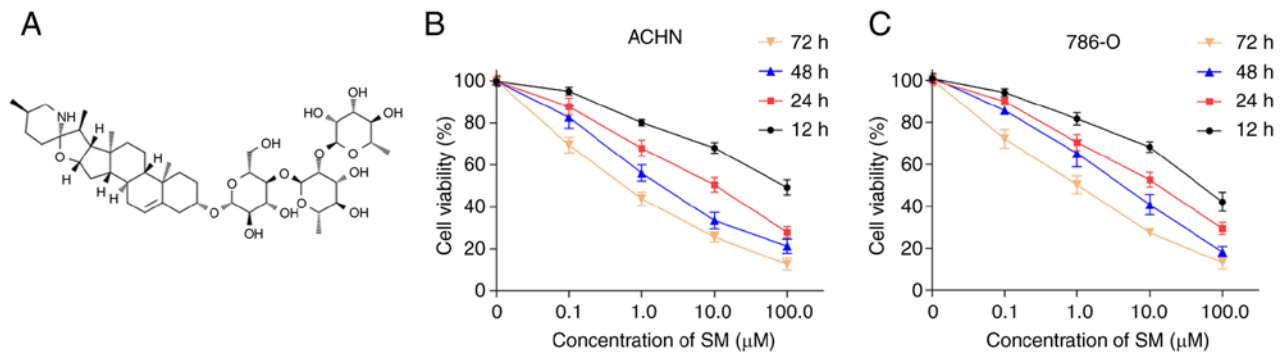


Figure 1. Effects of SM on the viability of ACHN and 786-O cells. (A) The chemical structure of SM. (B) ACHN and (C) 786-O cells were incubated with different concentrations of SM for 12, 24, 48 and 72 h. SM, solamargine.

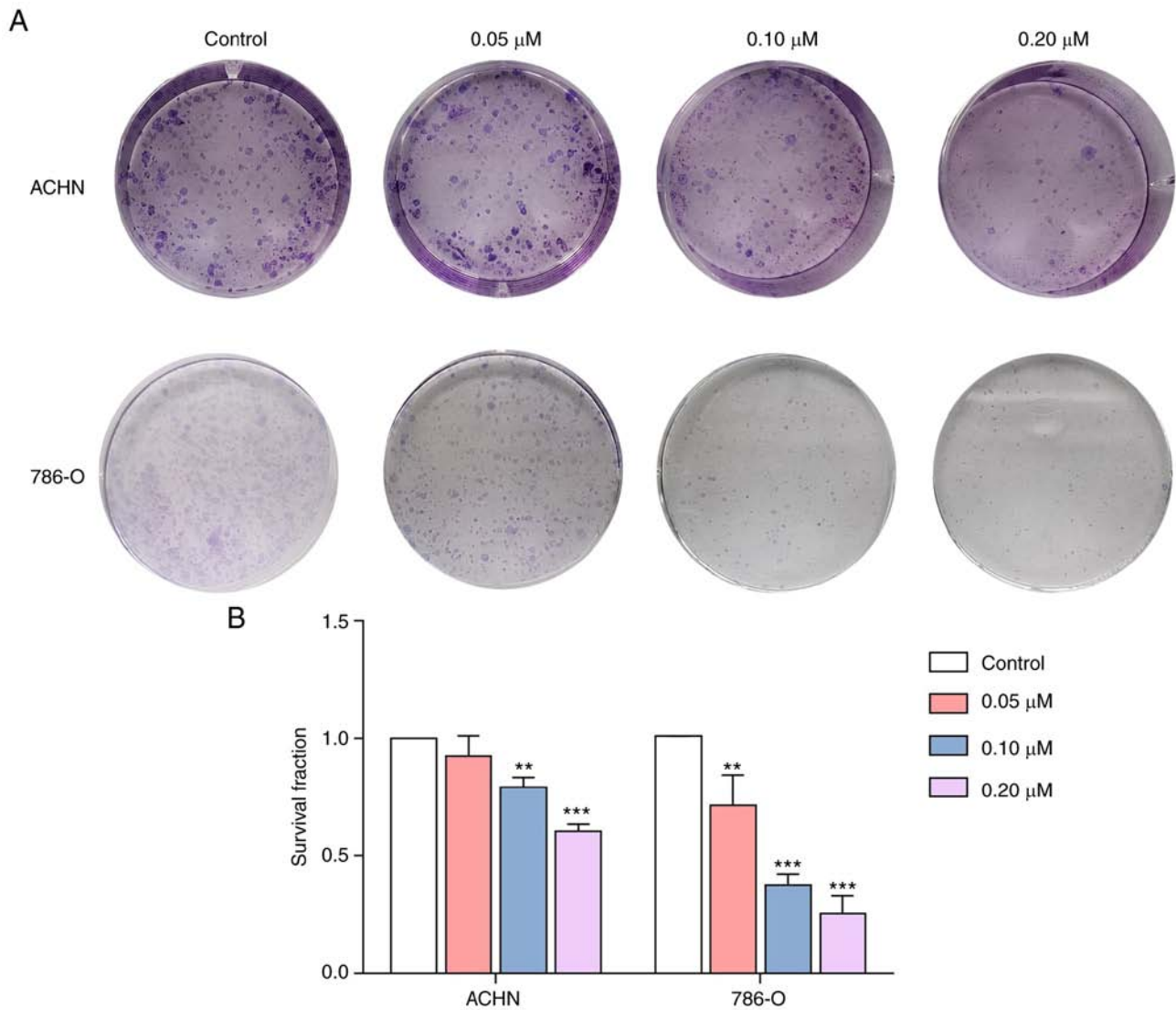


Figure 2. Effects of SM on the colony formation of ACHN and 786-O cells. (A) ACHN and 786-O cells were treated with different concentrations of SM [0 (control), 0.05, 0.10 and 0.20 μM] for 15 days. The resulting colonies were stained with Giemsa. (B) Survival fraction in treated ACHN and 786-O cells. ** $P < 0.01$, *** $P < 0.001$ vs. the control group. SM, solamargine.

SM inhibits tumor growth in ACHN xenograft mice. Whether SM could suppress tumor growth *in vivo* was next determined by analyzing its effect on an ACHN-bearing nude mouse model. Treatment with SM caused a significant decrease in

the volume and weight of tumor tissues (Fig. 7A-C) compared with the control group. Moreover, there was no significant difference in body weight between the experimental group and control group (Fig. 7D). H&E staining of the major organs

Table II. Effects of SM on the activities of caspases in treated 786-O and ACHN cells.

Cell line	SM concentration, μM	Caspase-3 activity, IU	Caspase-8 activity, IU	Caspase-9 activity, IU
786-O	0 (control)	1.800 \pm 0.081	1.757 \pm 0.095	1.367 \pm 0.100
	0.05	1.803 \pm 0.029	1.803 \pm 0.086	1.473 \pm 0.072
	0.10	2.133 \pm 0.116	1.897 \pm 0.110	1.657 \pm 0.215
	0.20	2.323 \pm 0.291 ^a	2.310 \pm 0.274 ^a	2.100 \pm 0.326 ^b
ACHN	0 (control)	2.183 \pm 0.144	1.507 \pm 0.111	1.803 \pm 0.127
	0.05	2.210 \pm 0.104	1.623 \pm 0.127	2.103 \pm 0.253
	0.10	2.597 \pm 0.038 ^a	1.770 \pm 0.085	2.367 \pm 0.093 ^a
	0.20	2.813 \pm 0.264 ^b	2.513 \pm 0.510 ^b	3.123 \pm 0.201 ^c

^aP<0.05, ^bP<0.01, ^cP<0.001 vs. the control group. SM, solamargine.

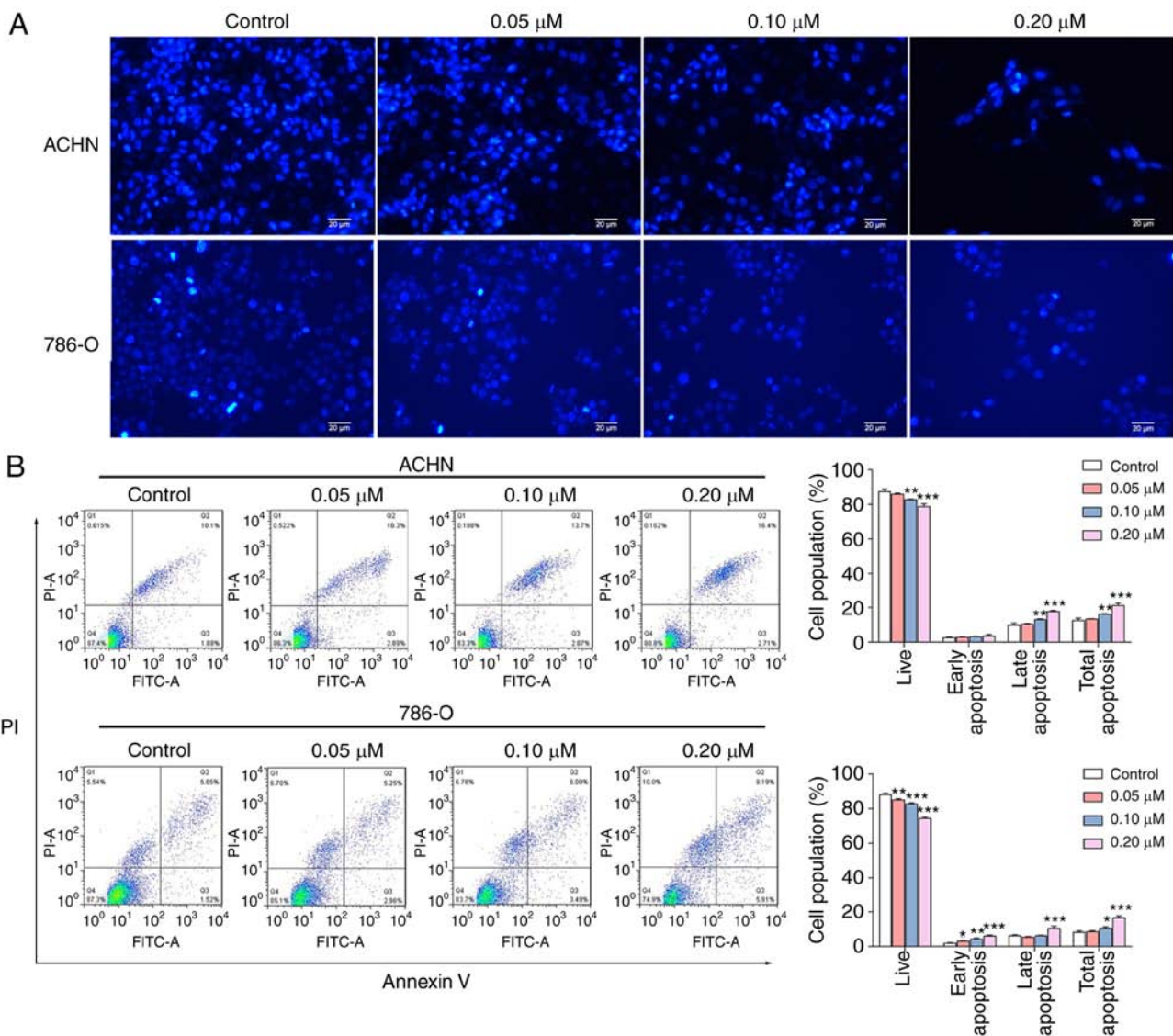


Figure 3. Effects of SM on the nucleus and apoptosis of ACHN and 786-O cells. (A) Morphological changes in nuclear chromatin following 24 h of SM treatment. (B) Cell apoptosis was analyzed via Annexin V/PI staining. Cells shown in the lower right and upper right represent the percentages of early and late apoptosis, respectively. ^{*}P<0.05, ^{**}P<0.01, ^{***}P<0.001 vs. the control group. PI, propidium iodide; SM, solamargine.

(heart, liver, spleen, lung and kidney) revealed no notable acute or chronic physiological toxicity following SM treatment

(Fig. 7E). Furthermore, SM treatment significantly decreased the number of p-STAT3⁺ cells compared with the control

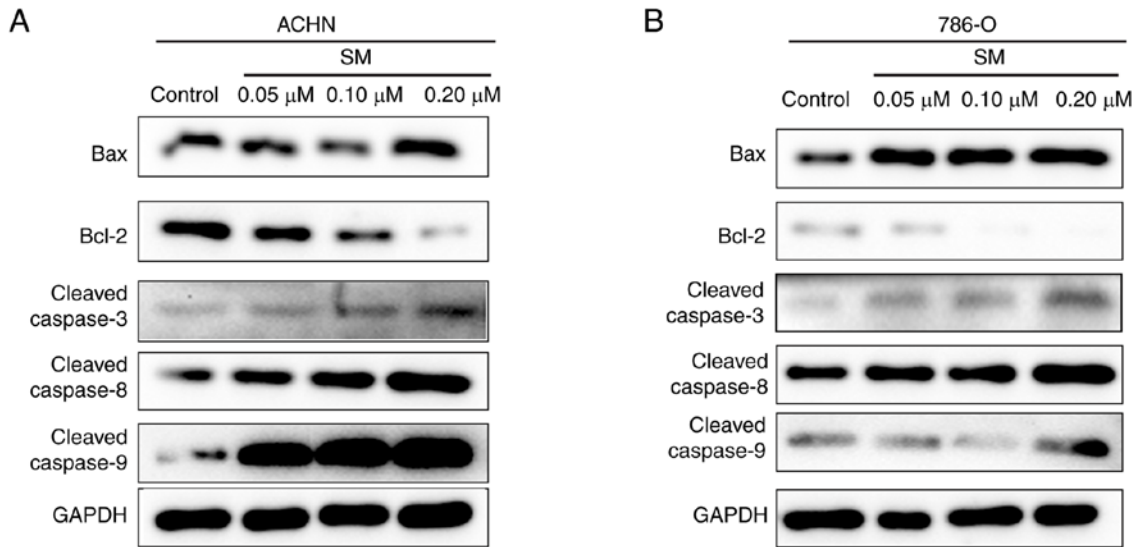


Figure 4. Effects of SM on expression of apoptosis-associated proteins in (A) ACHN and (B) 786-O cells. SM, solamargine.

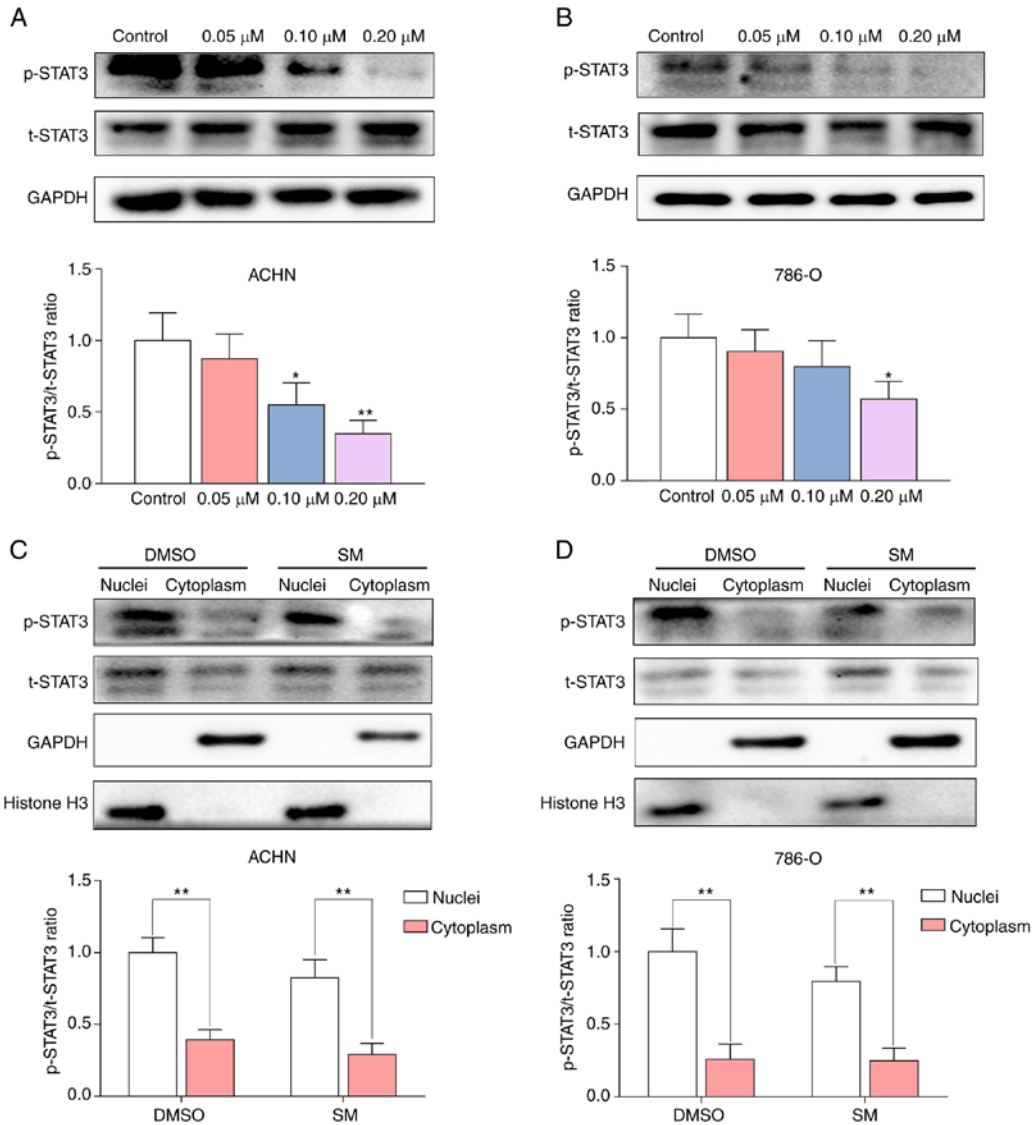


Figure 5. Effects of SM on the phosphorylation of STAT3 and its levels in the nuclei and cytoplasm of ACHN and 786-O cells. The impact of different SM doses on the p-STAT3/t-STAT3 ratio in (A) ACHN and (B) 786-O cells after treatment for 24 h. The nuclei and cytoplasm of (C) ACHN and (D) 786-O cells were fractionated after treatment with 0.20 μ M SM for 24 h, and the levels of p-STAT3 and t-STAT3 were detected. * P <0.05, ** P <0.01. DMSO, dimethyl sulfoxide; STAT3, signal transducer and activator of transcription-3; p-STAT3, phosphorylated STAT3, t-STAT3, total STAT3; SM, solamargine.

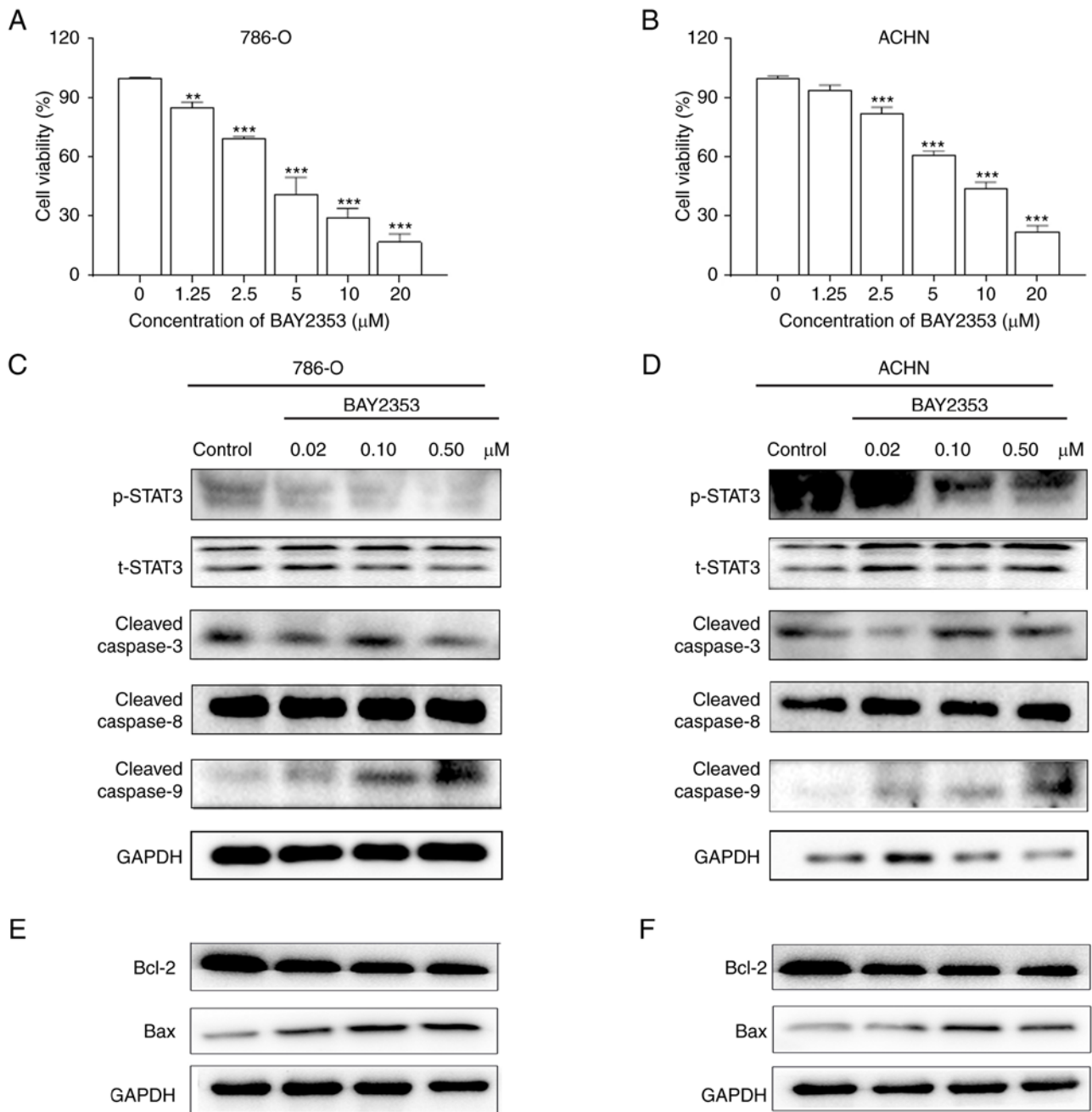


Figure 6. Effect of BAY2353 on cell viability and apoptosis-related proteins of renal cancer cells. Effects of BAY2353 on the proliferation of (A) 786-O and (B) ACHN cells. Effects of BAY2353 on the levels of STAT3, cleaved caspase-3, cleaved caspase-8 and cleaved caspase-9 in (C) 786-O and (D) ACHN cells. Effect of BAY2353 on the levels of Bcl-2 and Bax in (E) 786-O and (F) ACHN cells. ** $P < 0.01$, *** $P < 0.001$ vs. the control group. STAT3, signal transducer and activator of transcription-3; p-STAT3, phosphorylated STAT3, t-STAT3, total STAT3.

group, indicating that SM deactivated STAT3 phosphorylation in ACHN xenograft mice (Fig. 7F and G).

Discussion

RCC is the third most common malignant tumor of the urinary system (26). Although numerous treatment options exist for advanced RCC, the disease remains incurable. Notably, natural products have exhibited more favorable outcomes and lower side effects compared with chemical synthetic drugs, such as andrographis paniculata and phomaketides A (27-29). In the present study, results of the MTT assay revealed that

SM treatment inhibited RCC cell viability in a dose- and time-dependent manner, while findings from the colony formation assay indicated that SM inhibited the growth and clonogenicity of RCC cells in a dose-dependent manner. These results were consistent with previous studies that demonstrated that SM reduced the viability of various cancer cell types in a dose-dependent manner (15,30,31).

Apoptosis, a process of programmed cell death, occurs through both extrinsic and intrinsic pathways. While the extrinsic pathway is triggered by death receptors that result in caspase-8 activation, the intrinsic pathway is triggered by organelle injury leading to caspase-9 activation (32,33).

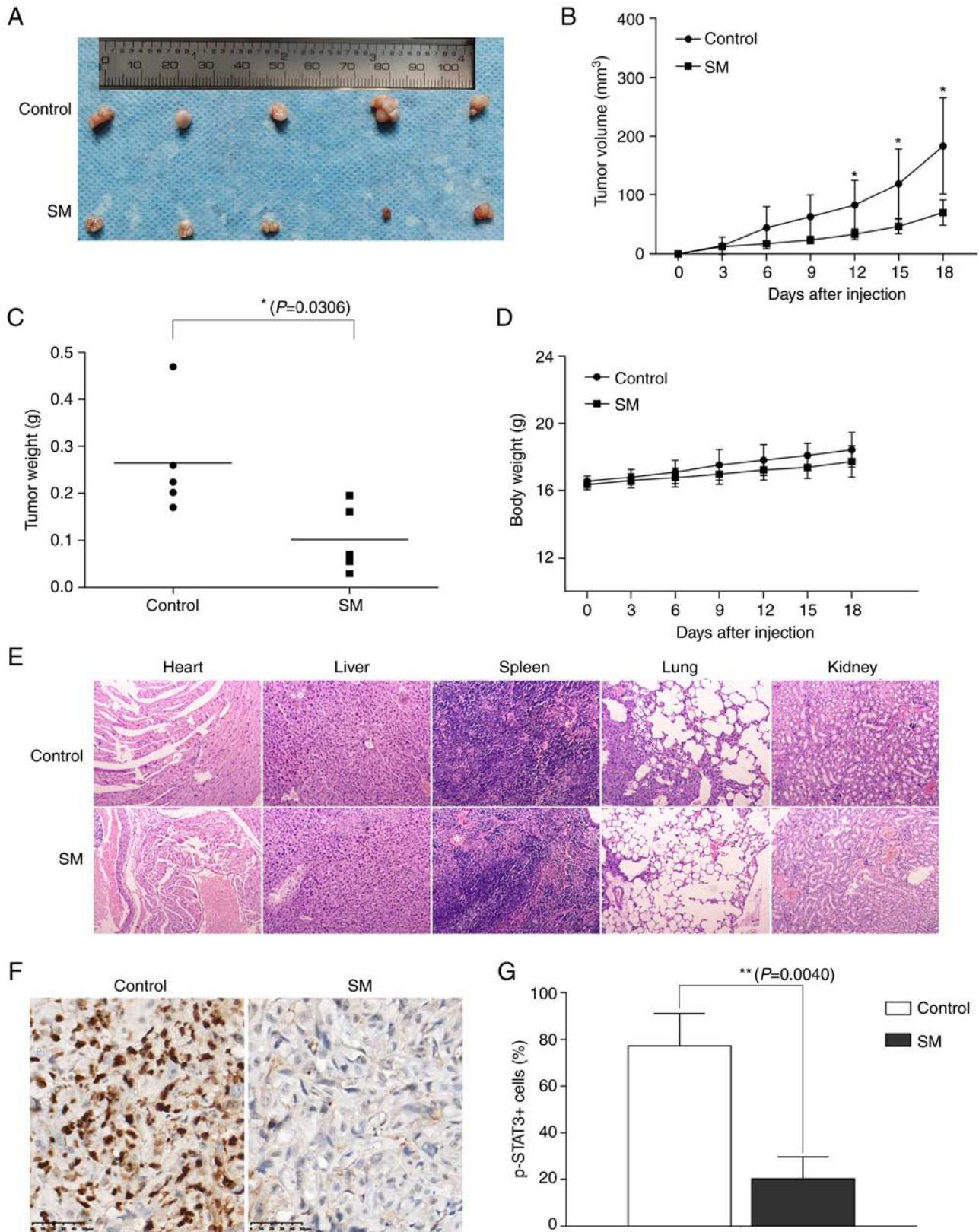


Figure 7. Effects of SM on tumor growth in ACHN-bearing nude mice. (A) tumors, (B) tumor volume, (C) tumor weight, (D) body weight, (E) Haematoxylin and eosin staining of major organs (heart, liver, spleen, lung and kidney) (x100) and (F) Immunohistochemical staining with the p-STAT3 antibody of tumor tissues from control and SM group mice (x400). (G) Quantification of pSTAT3⁺ cells. Data are presented as the mean \pm standard deviation, n=5. *P<0.05, **P<0.01 vs. control group. STAT3, signal transducer and activator of transcription-3; p-STAT3, phosphorylated STAT3, t-STAT3, total STAT3; SM, solamargine.

Both pathways have been shown to activate the same downstream caspase-3 molecules, to eventually trigger

cell apoptosis (25,34,35). Notably, the Bcl-2 family plays a critical role in controlling the intrinsic apoptotic pathway.

Both pathways have been previously reported in SM-induced apoptosis (25). Liang *et al* (36) found that tumor necrosis factor receptor 1-associated DEATH domain protein and FAS-associated death domain protein were recruited, while caspase-8 and caspase-3 were activated in SM-treated A549 cells. Moreover, it was demonstrated that SM treatment induced the release of cytochrome c from the mitochondria, downregulation of Bcl-2 and Bcl-x(L), upregulation of Bax and upregulation of caspase-9 activities in A549 cells (36). In addition, Xie *et al* (31) found that SM treatment mediated a significant downregulation of proliferation associated (Ki-67 and proliferating cell nuclear antigen) and anti-apoptotic (Bcl-2) proteins but promoted the activity of apoptosis-associated proteins (Bax, caspase-3 and caspase-9) in hepatocellular cells. Zhang *et al* (37) also reported that SM downregulated Bcl-2 and poly ADP ribose polymerase (PARP) proteins, but upregulated Bax, cleaved PARP, caspase 3, cleaved caspase 3 and caspase 7 proteins in QBC939 human cholangiocarcinoma cells. The results of the present study demonstrated that SM significantly increased apoptosis (accomplished by the upregulation of caspase-3, caspase-8, caspase-9 and Bax), whilst decreasing Bcl-2 levels in RCC cells. These results indicated that both the extrinsic and intrinsic pathways were involved in SM-induced apoptosis, which is consistent with previous studies.

A number of studies have reported the antitumor activities of SM. Notably, one study demonstrated that SM exerted its antitumor activity by inhibiting the MAPK signaling pathway (30), while another demonstrated that SM inhibited cell growth by suppressing PI3K/Akt signaling (15). In addition, Liu *et al* (38) concluded that the Notch signaling pathway was suppressed in SM-treated CM-319 human chordoma cells, while Zhou *et al* (39) demonstrated that SM not only inhibited proliferation but also induced the apoptosis of lung cancer cells through the p38 MAPK-mediated suppression of phosphorylation and protein expression of STAT3, followed by induction of the STAT3 downstream effector, p21. As a proto-oncogenic transcription factor, constitutive activation of STAT3 induces tumor development by promoting cell proliferation and inhibiting apoptosis (40,41). This implies that SM-mediated suppression of p-STAT3 may facilitate apoptosis. The results of the present study demonstrated that SM downregulated expression of p-STAT3 in a dose-dependent manner. Since tumor-promotion is ultimately regulated by STAT3-dependent transcriptional regulation of downstream oncogenes, the present study further focused on the localization of p-STAT3 and found that SM diminished its nuclear localization in cells. Therefore, it was hypothesized that SM suppressed translocation of STAT3 to the nucleus in RCC cells. These results indicated that the decreased p-STAT3 levels were associated with SM-induced apoptosis. Furthermore, intragastric administration of SM to ACHN-bearing nude mice at a ratio of 25 mg/kg suppressed tumor growth and decreased the number of p-STAT3⁺ cells in tumor tissue from the established xenograft mouse model, and it had no notable toxicity to the main organs. However, it is unclear whether higher SM drug concentrations will cause damages *in vivo*, and we will continue to explore in our further studies. In summary, the results of the present study indicated that SM triggered the apoptosis of RCC cells. This event was associated with the

inactivation of STAT3 phosphorylation. Taken together, these results indicated that SM has potential inhibitory effects on RCC cells and may be used in clinical practice in the future.

Acknowledgements

Not applicable.

Funding

This work was supported by grants from The Natural Science Foundation of Ningbo (grant nos. 202003N4295 and 2023J233), The General Health Foundation of Zhejiang Province (grant nos. 2021KY1067 and 2022KY1177), The Zhejiang Key Laboratory of Pathophysiology (grant no. 201910) and The Science and Technology Project of Yinzhou (grant nos. 2022AS033, 2023AS062 and 2023AS064).

Availability of data and materials

The datasets used and/or analyzed during the current study are available from the corresponding author on reasonable request.

Authors' contributions

DC, YR and GW designed the study. SH wrote the manuscript; SH, MS, TL and XW performed the experiments; XW analyzed the data. All authors read and approved the final version of the manuscript. SH, DC and GW confirm the authenticity of all the raw data.

Ethics approval and consent to participate

The animal study was approved by The Ethical Committee on Animal Research of Ningbo University (Ningbo, China; approval no. 10533).

Patient consent for publication

Not applicable.

Competing interests

The authors declare that they have no competing interests.

References

1. Siegel RL, Miller KD and Jemal A: Cancer statistics, 2020. *CA Cancer J Clin* 70: 7-30, 2020.
2. Capitanio U and Montorsi F: Renal cancer. *Lancet* 387: 894-906, 2016.
3. Huang J, Wang X, Wen G and Ren Y: miRNA2055p functions as a tumor suppressor by negatively regulating VEGFA and PI3K/Akt/mTOR signaling in renal carcinoma cells. *Oncol Rep* 42: 1677-1688, 2019.
4. Hillmer EJ, Zhang H, Li HS and Watowich SS: STAT3 signaling in immunity. *Cytokine Growth Factor Rev* 31: 1-15, 2016.
5. Sun Y, Liu L, Wang Y, He A, Hu H, Zhang J, Han M and Huang Y: Curcumin inhibits the proliferation and invasion of MG-63 cells through inactivation of the p-JAK2/p-STAT3 pathway. *Oncotargets Ther* 12: 2011-2021, 2019.
6. Song M, Wang C, Yang H, Chen Y, Feng X, Li B and Fan H: P-STAT3 inhibition activates endoplasmic reticulum stress-induced splenocyte apoptosis in chronic stress. *Front Physiol* 11: 680, 2020.

7. Tan B, Chen X, Fan Y, Yang Y, Yang J and Tan L: STAT3 phosphorylation is required for the HepaCAM-mediated inhibition of castration-resistant prostate cancer cell viability and metastasis. *Prostate* 81: 603-611, 2021.
8. Zhang ZH, Li MY, Wang Z, Zuo HX, Wang JY, Xing Y, Jin C, Xu G, Piao L, Piao H, *et al*: Convallatoxin promotes apoptosis and inhibits proliferation and angiogenesis through crosstalk between JAK2/STAT3 (T705) and mTOR/STAT3 (S727) signaling pathways in colorectal cancer. *Phytomedicine* 68: 153172, 2020.
9. Jahangiri A, Dadmanesh M and Ghorban K: STAT3 inhibition reduced PD-L1 expression and enhanced antitumor immune responses. *J Cell Physiol* 235: 9457-9463, 2020.
10. Lorente D, Arevalo J, Salcedo MT, Trilla E, de Torres I, Meseguer A and Morote J: Analysis of the nuclear expression of pSer727-STAT3 as a prognostic factor in patients with clear cell renal carcinoma. *Actas Urol Esp (Engl Ed)* 44: 245-250, 2020 (In English, Spanish).
11. Zhan C, Xu C, Chen J, Shen C, Li J, Wang Z, Ying X, Luo Z, Ren Y, Wu G, *et al*: Development and Validation of an IL6/JAK/STAT3-Related gene signature to predict overall survival in clear cell renal cell carcinoma. *Front Cell Dev Biol* 9: 686907, 2021.
12. Arevalo J, Lorente D, Trilla E, Salcedo MT, Morote J and Meseguer A: Nuclear and cytosolic pS727-STAT3 levels correlate with overall survival of patients affected by clear cell renal cell carcinoma (ccRCC). *Sci Rep* 11: 6957, 2021.
13. Lorente D, Trilla E, Meseguer A, Arevalo J, Nemours S, Planas J, Placer J, Celma A, Salvador C, Regis L, *et al*: The role of STAT3 protein as a prognostic factor in the clear cell renal carcinoma. Systematic review. *Actas Urol Esp (Engl Ed)* 43: 118-123, 2019 (In English, Spanish).
14. Li S, Priceman SJ, Xin H, Zhang W, Deng J, Liu Y, Huang J, Zhu W, Chen M, Hu W, *et al*: Icaritin inhibits JAK/STAT3 signaling and growth of renal cell carcinoma. *PLoS One* 8: e81657, 2013.
15. Ge J, Wang P, Ma H and Zhang J: Solamargine inhibits prostate cancer cell growth and enhances the therapeutic efficacy of docetaxel via Akt signaling. *J Oncol* 2022: 9055954, 2022.
16. Sani IK, Marashi SH and Kalalinia F: Solamargine inhibits migration and invasion of human hepatocellular carcinoma cells through down-regulation of matrix metalloproteinases 2 and 9 expression and activity. *Toxicol In Vitro* 29: 893-900, 2015.
17. Furtado RA, Ozelin SD, Ferreira NH, Miura BA, Almeida Junior S, Magalhaes GM, Nassar EJ, Miranda MA, Bastos JK and Tavares DC: Antitumor activity of solamargine in mouse melanoma model: Relevance to clinical safety. *J Toxicol Environ Health A* 85: 131-142, 2022.
18. Wu YH, Chiu WT, Young MJ, Chang TH, Huang YF and Chou CY: Solanum Incanum extract downregulates aldehyde dehydrogenase I-mediated stemness and inhibits tumor formation in ovarian cancer cells. *J Cancer* 6: 1011-1019, 2015.
19. Al Chami L, Mendez R, Chataing B, O'Callaghan J, Usubillaga A and Lacruz L: Toxicological effects of alpha-solamargine in experimental animals. *Phytother Res* 17: 254-258, 2003.
20. Sezer ED, Oktay LM, Karadadas E, Memmedov H, Selvi Gunel N and Sozmen E: Assessing anticancer potential of blueberry flavonoids, quercetin, kaempferol, and genticic acid, through oxidative stress and apoptosis parameters on HCT-116 cells. *J Med Food* 22: 1118-1126, 2019.
21. Wang HQ, Man QW, Huo FY, Gao X, Lin H, Li SR, Wang J, Su FC, Cai L, Shi Y, *et al*: STAT3 pathway in cancers: Past, present, and future. *MedComm (2020)* 3: e124, 2022.
22. Fan M, Sun W, Gu X, Lu S, Shen Q, Liu X and Zhang X: The critical role of STAT3 in biogenesis of tumor-derived exosomes with potency of inducing cancer cachexia in vitro and in vivo. *Oncogene* 41: 1050-1062, 2022.
23. Qin JJ, Yan L, Zhang J and Zhang WD: STAT3 as a potential therapeutic target in triple negative breast cancer: A systematic review. *J Exp Clin Cancer Res* 38: 195, 2019.
24. Liu Y, Liao S, Bennett S, Tang H, Song D, Wood D, Zhan X and Xu J: STAT3 and its targeting inhibitors in osteosarcoma. *Cell Prolif* 54: e12974, 2021.
25. Yang J, Ren Y, Lou ZG, Wan X, Weng GB and Cen D: Paconiflorin inhibits the growth of bladder carcinoma via deactivation of STAT3. *Acta Pharm* 68: 211-222, 2018.
26. Deleuze A, Saout J, Dugay F, Peyronnet B, Mathieu R, Verhoest G, Bensalah K, Crouzet L, Laguerre B, Belaud-Rotureau MA, *et al*: Immunotherapy in Renal cell carcinoma: The future is now. *Int J Mol Sci* 21: 2532, 2020.
27. Islam MR, Akash S, Rahman MM, Nowrin FT, Akter T, Shohag S, Rauf A, Aljohani ASM and Simal-Gandara J: Colon cancer and colorectal cancer: Prevention and treatment by potential natural products. *Chem Biol Interact* 368: 110170, 2022.
28. Shams Ul Hassan S, Ishaq M, Zhang WD and Jin HZ: An overview of the mechanisms of marine fungi-derived anti-inflammatory and anti-tumor agents and their novel role in drug targeting. *Curr Pharm Des* 27: 2605-2614, 2021.
29. Su M, Qin B, Liu F, Chen Y and Zhang R: Andrographolide enhanced 5-fluorouracil-induced antitumor effect in colorectal cancer via inhibition of c-MET pathway. *Drug Des Devel Ther* 11: 3333-3341, 2017.
30. Fu R, Wang X, Hu Y, Du H, Dong B, Ao S, Zhang L, Sun Z, Zhang L, Lv G and Ji J: Solamargine inhibits gastric cancer progression by regulating the expression of lncNEAT1_2 via the MAPK signaling pathway. *Int J Oncol* 54: 1545-1554, 2019.
31. Xie X, Zhu H, Yang H, Huang W, Wu Y, Wang Y, Luo Y, Wang D and Shao G: Solamargine triggers hepatoma cell death through apoptosis. *Oncol Lett* 10: 168-174, 2015.
32. Porubsky M, Reznickova E, Krupkova S, Krystof V and Hlavac J: Development of fluorescent dual-FRET probe for simultaneous detection of caspase-8 and caspase-9 activities and their relative quantification. *Bioorg Chem* 129: 106151, 2022.
33. Mcglorthan L, Paucarmayta A, Casablanca Y, Maxwell GL and Syed V: Progesterone induces apoptosis by activation of caspase-8 and calcitriol via activation of caspase-9 pathways in ovarian and endometrial cancer cells in vitro. *Apoptosis* 26: 184-194, 2021.
34. Goldar S, Khaniani MS, Derakhshan SM and Baradaran B: Molecular mechanisms of apoptosis and roles in cancer development and treatment. *Asian Pac J Cancer Prev* 16: 2129-2144, 2015.
35. Jin Z and El-Deiry WS: Overview of cell death signaling pathways. *Cancer Biol Ther* 4: 139-163, 2005.
36. Liang CH, Liu LF, Shiu LY, Huang YS, Chang LC and Kuo KW: Action of solamargine on TNFs and cisplatin-resistant human lung cancer cells. *Biochem Biophys Res Commun* 322: 751-758, 2004.
37. Zhang X, Yan Z, Xu T, An Z, Chen W, Wang X, Huang M and Zhu F: Solamargine derived from Solanum nigrum induces apoptosis of human cholangiocarcinoma QBC939 cells. *Oncol Lett* 15: 6329-6335, 2018.
38. Liu J, Wang Z, Xu C, Qi Y and Zhang Q: Solamargine inhibits proliferation and promotes apoptosis of CM-319 human chordoma cells through suppression of notch pathway. *Transl Cancer Res* 8: 509-519, 2019.
39. Zhou Y, Tang Q, Zhao S, Zhang F, Li L, Wu W, Wang Z and Hann S: Targeting signal transducer and activator of transcription 3 contributes to the solamargine-inhibited growth and -induced apoptosis of human lung cancer cells. *Tumour Biol* 35: 8169-8178, 2014.
40. Mohassab AM, Hassan HA, Abdelhamid D and Abdel-Aziz M: STAT3 transcription factor as target for anti-cancer therapy. *Pharmacol Rep* 72: 1101-1124, 2020.
41. Fathi N, Rashidi G, Khodadadi A, Shahi S and Sharifi S: STAT3 and apoptosis challenges in cancer. *Int J Biol Macromol* 117: 993-1001, 2018.

